

Supporting Information

Management of Intermediate Phase via a Multifunctional Dietary Supplement for Efficient and Stable Perovskite Solar Cells

Chuizheng Feng,^{#a,b} Jia Yang,^{#a,b} Shungao Yin,^{#b} Gang Xie,^{a,b} Mengqing Wang,^b Jianxing Yu,^{a,b} Ruonan Zhao,^{a,b} Yang Pan,^b Aihui Liang,^{*a,b} and Yiwang Chen^{*a,c}

Experimental Section

Materials: All chemicals and reagents are purchased and used directly without further purification. N, N-dimethylformamide (DMF, anhydrous, 99.8%), dimethyl sulfoxide (DMSO, anhydrous, ≥99.9%), chlorobenzene (CB, 99.8%), acetonitrile (99.8%), bis (trifluoromethane) sulfonimide lithium salt (Li-TSFI, 99.95%), 4-tert-butylpyridine (*t*BP, 96%) and bathocuproine (BCP, 96.0%) were purchased from Sigma-Aldrich. Tin oxide (SnO₂, 15% in H₂O colloidal dispersion) colloid precursor and lead iodide (PbI₂, 99.999%) were purchased from Alfa Aesar. Formamidinium iodide (FAI, 99.5%), methyl bromide (MABr, 99.5%), methylamine hydrochloride (MACl, 99.5%), cesium iodide (CsI, 99.9%) and phenyl-C₆₁-butyric acid methyl ester (PC₆₁BM, 99.5%) were purchased from Xi'an Polymer Light Technology Corp. 2,2',7,7'-tetrakis(N,N-di-p-methoxyphenylamine)-9,9-spirobifluorene (Spiro-OMeTAD, 99.5%) was purchased from Luminescence Technology Corp. Glucosamine hydrochloride (GluACl, 99%) was purchased from J&K scientific.

Synthesis of (GluA)(PbI₃)·3DMSO single crystals: PbI₂ and GluAI (1/1 by molar, 0.1 M) were dissolved in 200 μL DMSO and overnight at 100 °C. The containing solution vial was then placed into a sealed bottle filled with 1 mL CB and 1mL CF. The (GluA)(PbI₃)·3DMSO single crystals were grown along with the slow diffusion of the vapour of the antisolvent CB and CF into the solution.

Precursor solution: Precursor solution based on Cs_{0.05}(FA_{0.83}MA_{0.17})_{0.95}Pb(I_{0.9}Br_{0.1})₃ was prepared by mixing 742.2 mg PbI₂, 224.4 mg FAI, 16.2 mg MABr, 13.5 mg MACl and 19.8 mg CsI powder in DMF/DMSO (4:1, v/v) with stirring 2 h at 60 °C before used. Spiro-OMeTAD (72.3 mg/mL) solution was prepared by dissolving into CB, as well as containing *t*BP (28.8 μL) and Li-TSFI solution (17.5 μL, 520 mg/mL in acetonitrile).

Fabrication of perovskite solar cells: Indium tin oxide (ITO) glass substrates were cleaned with ultrasonic treatment in acetone, detergent, deionized water and isopropyl alcohol for 20 min and then the substrates were dried by nitrogen flow. The substrates were then treated in a plasma cleaning machine for 3 min. For the n-i-p device with structure of ITO/SnO₂/perovskite/spiro-OMeTAD/Ag, SnO₂ (diluted by H₂O to 2.67%) was first spin-coated on ITO at 3000 rpm for 30 s, and transferred into N₂ glove box after a thermal annealing (150°C for 30 min) in air. Then the perovskite precursor solution was spin coated onto the SnO₂ layer at 1000 rpm for 10 s and 5000 rpm for 30 s, following with 0.15 mL dropping of CB anti-solvent in the last 7 s. The substrate was then heated at 150°C for 10 min to form perovskite films. After the substrate cooled to room-temperature, Spiro-OMeTAD solution was spin-coated on perovskite films at 3000 rpm for 30 s. Finally, a 100 nm Ag was deposited by thermal evaporation as the metal electrode (rate of 1.0 Å/s).

Device characterization: The current density-voltage (J - V) characteristics were measured by a Keithley 2400 Source Meter (Enlitech, QE-R3011) under simulated solar light (100 mW/cm², AM 1.5 G, Abet Solar Simulator Sun2000). The external quantum efficiency (EQE) spectra were recorded on a commercial EQE measurement system (Enlitech, QE-R3011). Highly sensitive EQE was measured using an integrated system (PECT-600, Enlitech), where the photocurrent was amplified and modulated by a lock-in instrument. EQE_{EL} measurements were performed by applying external voltage/current sources through the devices (ELCT-3010, Enlitech). A digital oscilloscope acquired the TPV signal at the open-circuit condition. An optical perturbation is applied to the device with a 1 kHz femtosecond pulse laser under 640 nm excitation. TPC signal was measured under approximately short-circuit conditions by applying a 100 Ω resistor. Electrical impedance spectroscopy (EIS) of PVSCs was tested in a frequency range from 1 MHz to 10 MHz by using Zahner electrochemical workstation under dark conditions. EQE_{EL} measurements were carried out from 1.2 to 2 V. The devices were mounted on a conductive clip and under steady-state illumination from a focused Quartz Tungsten-Halogen Lamp light source. The analyses were performed with a background response similar to open-circuit voltage. The thermal stability of the devices was characterized by testing the normalized PCE decay of the unpackaged PVSCs kept in N₂ atmosphere at 85 °C over 1000 h, with PCE tested every 120 hours. The curve of V_{OC} and J_{SC} light intensity dependence fitting equation can be express as $V_{OC} = nKT/q\ln(P_{light})$ and $\log J_{SC} = \alpha\log P_{light}$, where k is Boltzmann's constant, T is the absolute temperature, q is elementary charge.

Material Characterization: Unless otherwise specified, all films were characterized in ambient atmosphere (25 °C, 20-30% RH). The crystallization process of perovskite was studied by in situ Ultraviolet-visible (UV-vis) and in situ photoluminescence (PL) measurements using in Hot Station Spectrometer (TU-100, Shaanxi Spectral light micro vision Technology Co. LTD). Scanning electron microscopy (SEM) images were obtained by a SU8020 scanning electron microscope with 8 kV

acceleration voltage. Atomic force microscopy (AFM) images were obtained by a Bruker Dimension Icon instrument (USA). Transmission electron microscopy (TEM) images were taken on a JEM2100 transmission electron microscope and an internal charge-coupled device (CCD) camera. X-ray diffraction (XRD) patterns were tested on a Rigaku D/Max-B X-ray diffractometer with Bragg-Brentano parafocusing geometry to reflect the crystallinity of the single crystal or perovskite films. GIWAXS measurements were carried out with a Xeuss 2.0 SAXS/WAXS laboratory beamline using a Cu X-ray source (8.05 keV, 1.54 Å) and a Pilatus3R 300K detector. UV-visible absorption spectra were acquired on a PerkinElmer LAMBDA 1050+ instrument. Fourier transform infrared (FTIR) spectra were recorded with PerkinElmer Spectrum One infrared spectrophotometer using KBr sheets. Nuclear magnetic resonance spectra were recorded on (Bruker Avance 400). X-ray photoelectron spectroscopy (XPS) and ultraviolet photoelectron spectroscopy (UPS) was performed on a photoelectron spectrometer (Thermo Fischer ESCALAB 250Xi). High-sensitivity steady-state transient fluorescence spectrometer Horiba QM8000 was applied to investigate the steady-state photoluminescence (PL) and time-resolved photoluminescence (TRPL) of perovskite films. Contact angle measurements of films were performed at a Krüss DSA100s Drop Shape Analyzer. Water was used as probe liquids. Confocal laser scanning microscope (CLSM) was detected by FastFLIM-Q2 by ISS (Champaign Illinois, USA). The specimen for PL measurements was prepared using the same procedures for device preparation but without Spiro-OMeTAD/Ag on top of the active layer and SnO₂ on buried interface. For PL measurements, two (532 nm) lasers are pulsed at 10 MHz. The PL lifetime is obtained by double-exponential fitting.

DFT calculations: The DFT calculations were performed with a plane wave method implemented in the Quantum-Espresso package.^{S1} The exchange correlation was evaluated through the generalized gradient approximation (GGA) with the Perdew-Burke-Ernzerh (PBE) functional. Pseudopotentials from the well-established SSSP library (version 1.1) were exclusively employed.^{S2} Energy cutoffs of 60 and 480 Rydberg were chosen for wavefunction and charge density expansion, and the Hellmann-Feynman forces converged below 0.01 eV Å⁻¹ for structural optimizations. The convergence criteria of the electronic wave function were 1.0×10^{-6} eV. Van der Waals interactions were included via Grimme's DFT-D3 scheme.^{S3} The k-mesh sampling was defined such that the k-spacing became less than 0.12 Å⁻¹ for both 3D and 2D crystals. For the calculation of the gas-phase molecule, only Γ -point was included in the k-mesh sampling. Slab calculations employed a vacuum of at least 15 Å to avoid the interaction between neighboring interfaces along the z-direction. The formation energy of the intermediate phase (GluA)(PbI₃)·3DMSO was determined using the equation $\Delta E_{(\text{GluA})(\text{PbI}_3)\cdot 3\text{DMSO}} = E_{\text{GluA}} - E_{\text{PbI}_2} - 2E_{\text{DMSO}}$, corresponding to the reaction $\text{PbI}_2 + \text{GluA} + 2\text{DMSO} \rightarrow (\text{GluA})(\text{PbI}_3)\cdot 3\text{DMSO}$. For the gas-phase GluA-PbI₂ formation, the formation energy was calculated by $\Delta E_{\text{GluAI-PbI}_2} = E_{\text{GluAI}} - E_{\text{PbI}_2}$ for the reaction $\text{PbI}_2 + \text{GluA} \rightarrow \text{GluA-PbI}_2$. Similarly, the formation

energy of δ -FAPbI₃ was calculated using the equation $\Delta E_{\delta\text{-FAPbI}_3} = E_{\text{FAI}} - E_{\text{PbI}_2}$, which pertains to the reaction $\text{PbI}_2 + \text{FAI} \rightarrow \delta\text{-FAPbI}_3$. The gaseous state of reactants served as the reference state. The electrostatic potentials (ϕ), and dipoles moment of molecules were computed using the ORCA program at the B3LYP/def2TZVP level with DFT-D3.^{S4} Electron Localization Function (ELF) was obtained from the multiwfn program^{S5} and visualized in ChimeraX^{S6}. Prior to initiating ab initio molecular dynamics (AIMD) simulations, the initial atomic positions were optimized by the Quantum Espresso code with GGA-PBE functional. The AIMD simulations were performed utilizing the SIESTA code with local NAO basis sets and GGA-PBE pseudopotentials.^{S7} Additional information regarding pseudopotential generation and basis optimization can be found in the reference.^{S8} The AIMD simulations were carried out under the canonical ensemble (NVT ensemble) employing the Nose-Hoover thermostat with 1 fs as a temporal step at the fixed temperature of 300 K.

[CCDC 2299758 contains the supplementary crystallographic data for this paper. These data can be obtained free of charge from The Cambridge Crystallographic Data Centre via www.ccdc.cam.ac.uk/data_request/cif.]

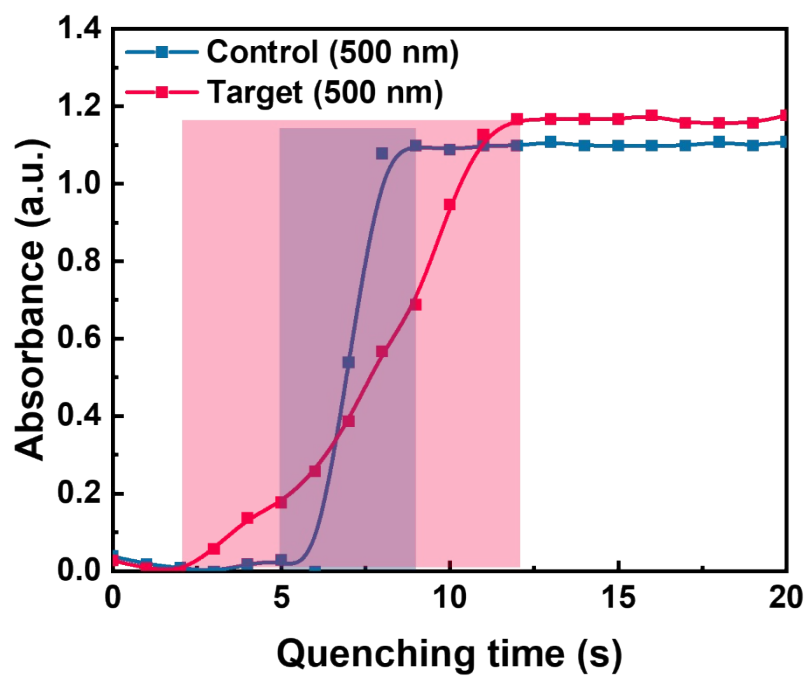


Figure S1. UV-vis absorption intensity at the wavelength of 500 nm as a function of annealing time for control and target perovskite films.

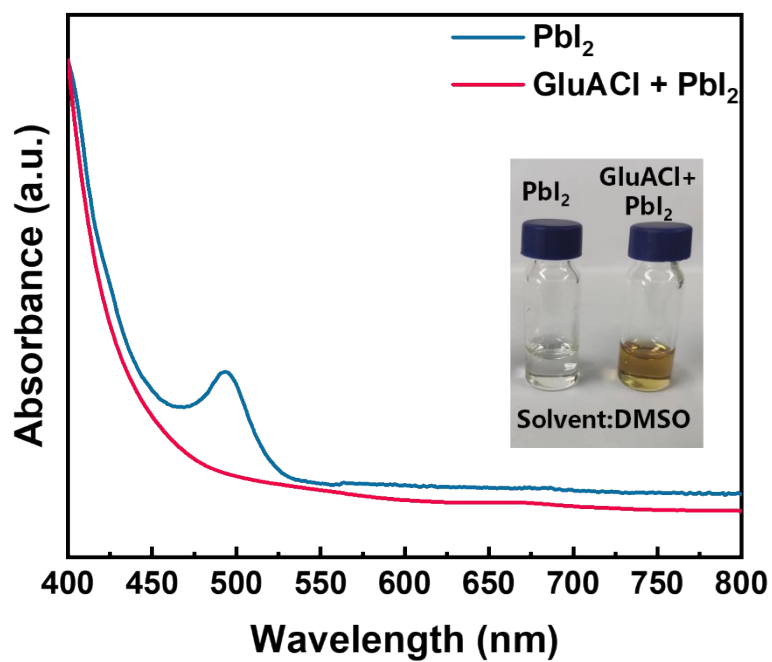


Figure S2. UV-vis absorption spectra of PbI_2 solutions without and with GluACI (inset: photographs of the corresponding solution).

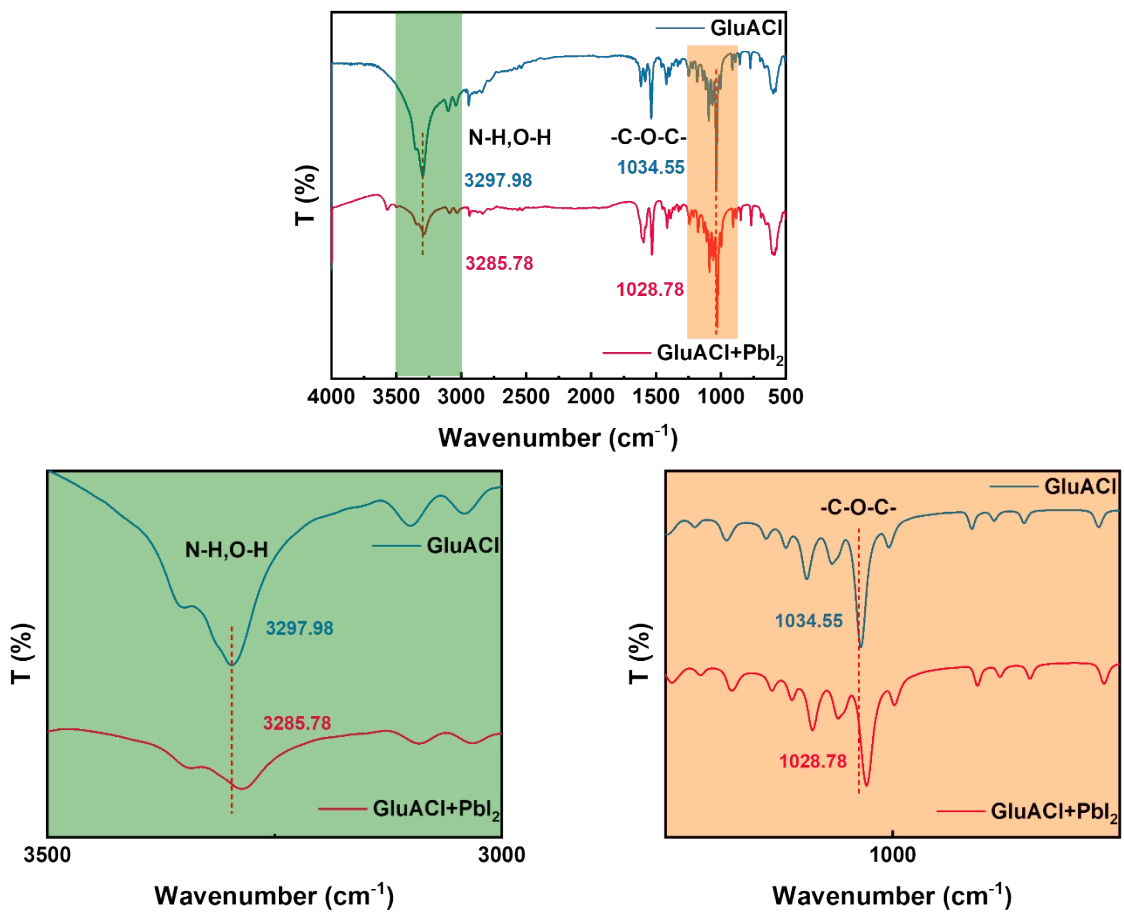


Figure S3. FTIR spectra of GluACl and GluACl containing PbI₂ solutions.

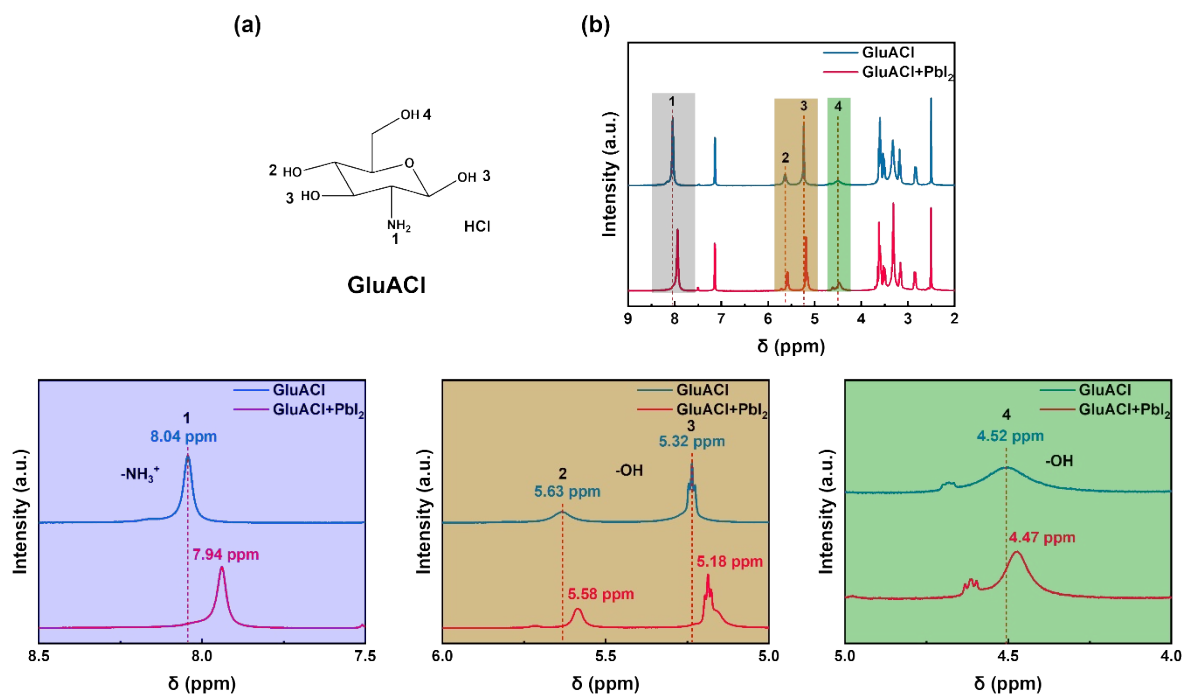


Figure S4. (a) Structural formula of GluACl. (b) ¹H NMR spectra of GluACl and GluACl containing PbI₂ solutions.

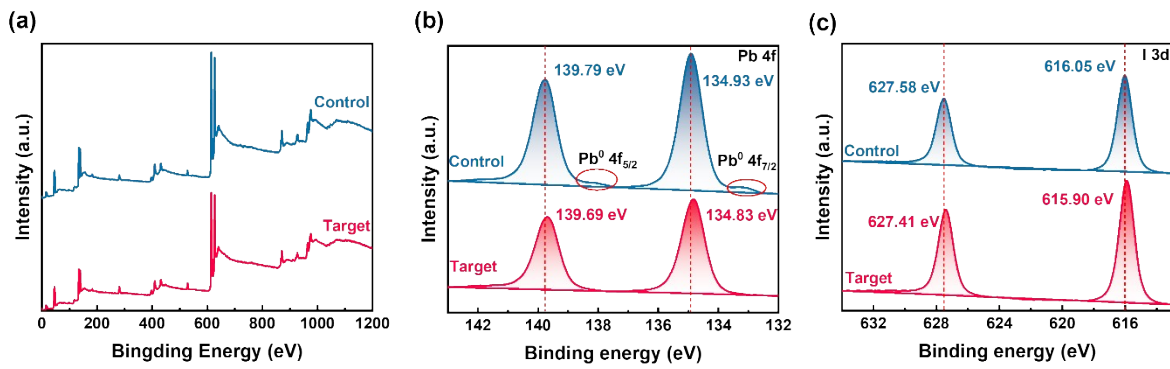


Figure S5. (a) All XPS spectra and XPS spectra of (b) Pb 4f and (c) I 3d based on control and target films.

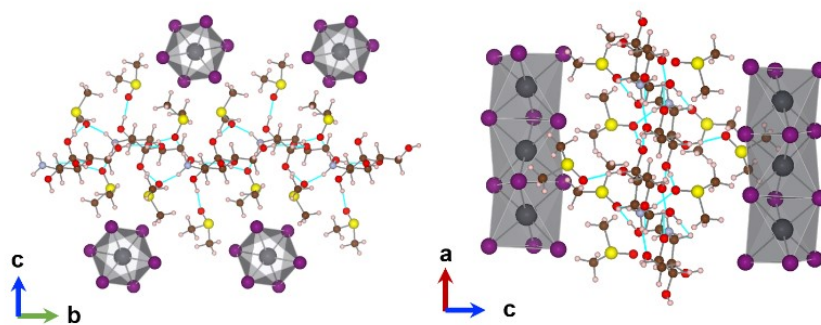


Figure S6. Crystal structure of the intermediate phase $(\text{GluA})(\text{PbI}_3) \cdot 3\text{DMSO}$, where hydrogen bondings are highlighted in cyan.

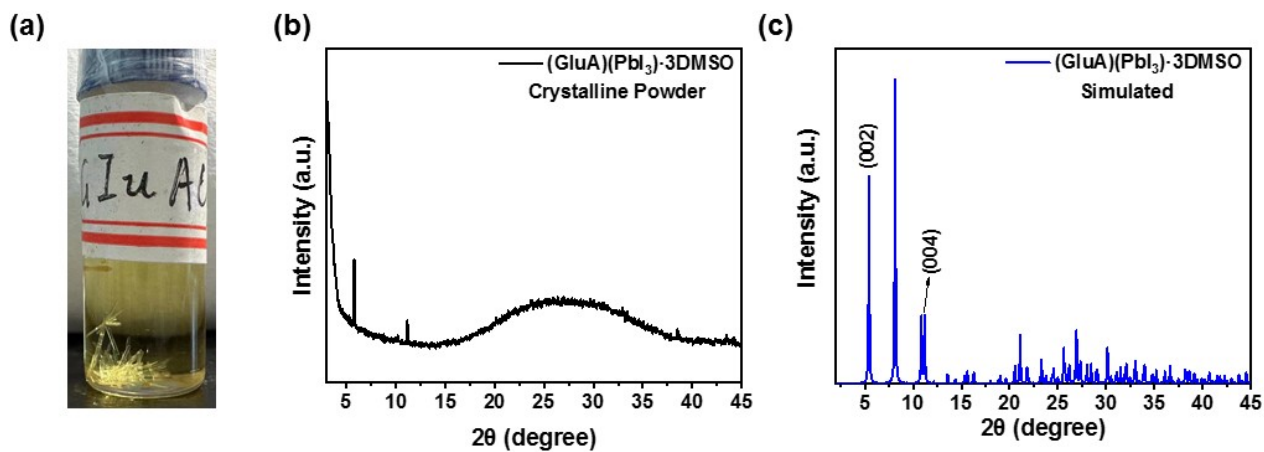


Figure S7. (a) Transparent (GluA)(PbI₃)·3DMSO crystals. The experimental crystalline powder (b) and simulated (c) XRD of the (GluA)(PbI₃)·3DMSO single crystal.

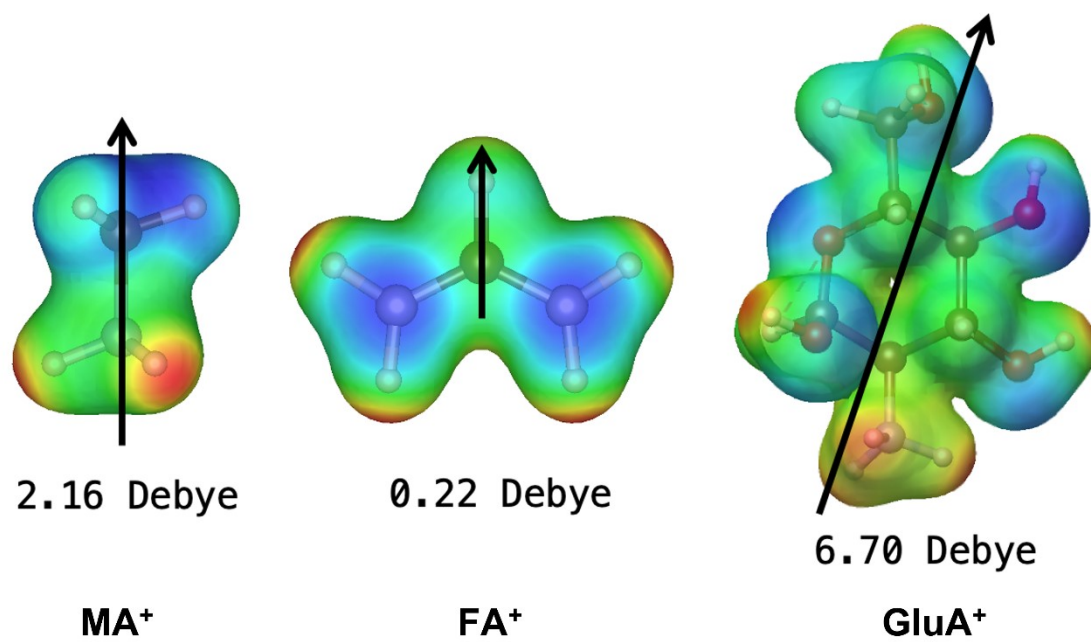


Figure S8. The dipole moments of MA⁺, FA⁺ and GluA⁺.

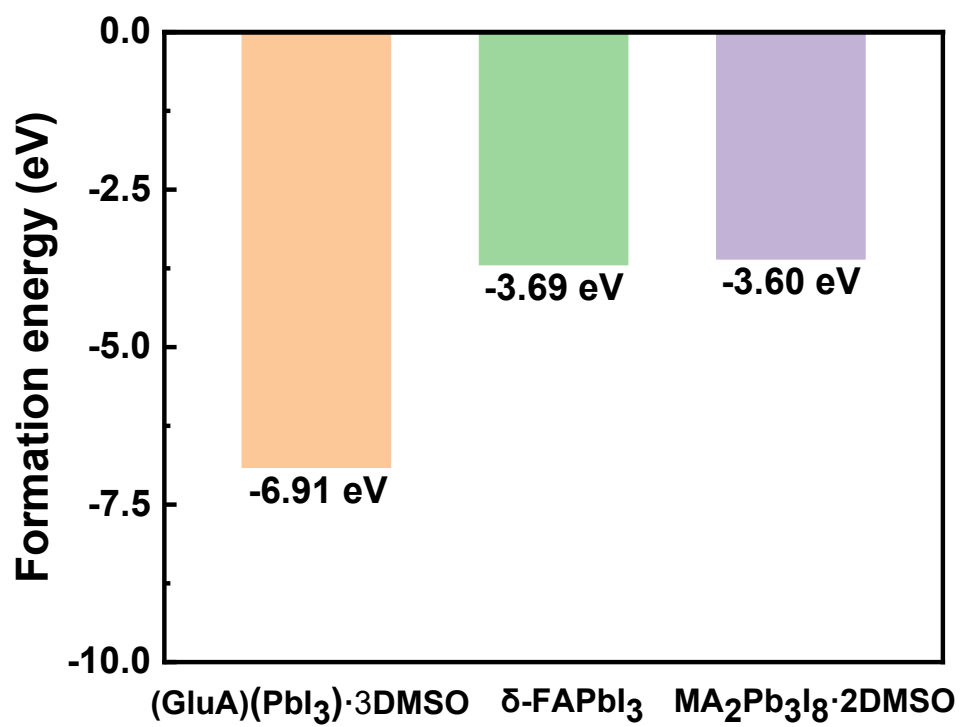


Figure S9. Formation energies of (GluA)(PbI₃)·3DMSO, δ-FAPbI₃ and MA₂Pb₃I₈·2DMSO.

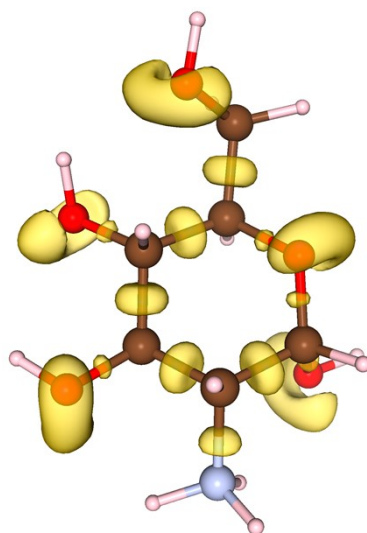


Figure S10. ELF representation of GluA⁺ (in cyan color, isovalue = 0.85), where ELF around H atoms are hidden.

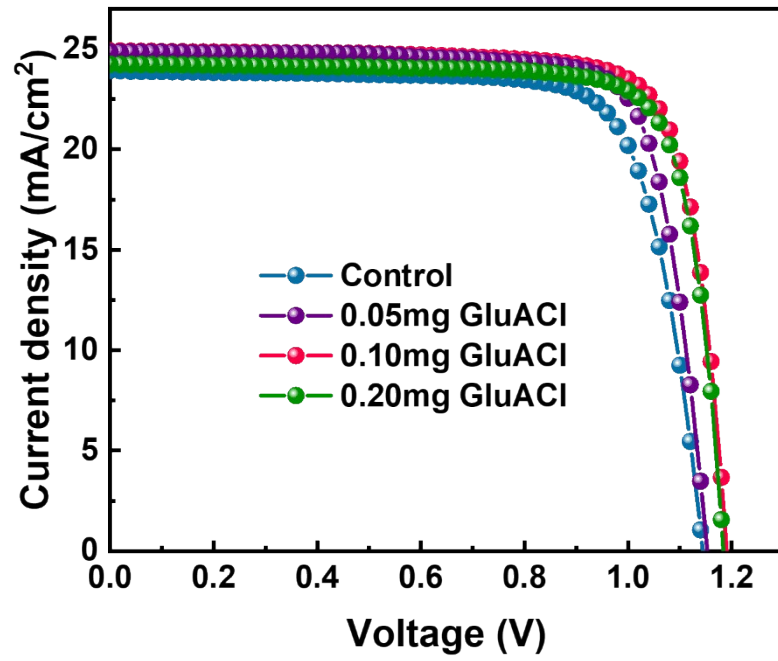


Figure S11. J - V for the devices based on the perovskite films with different GluACl concentrations.

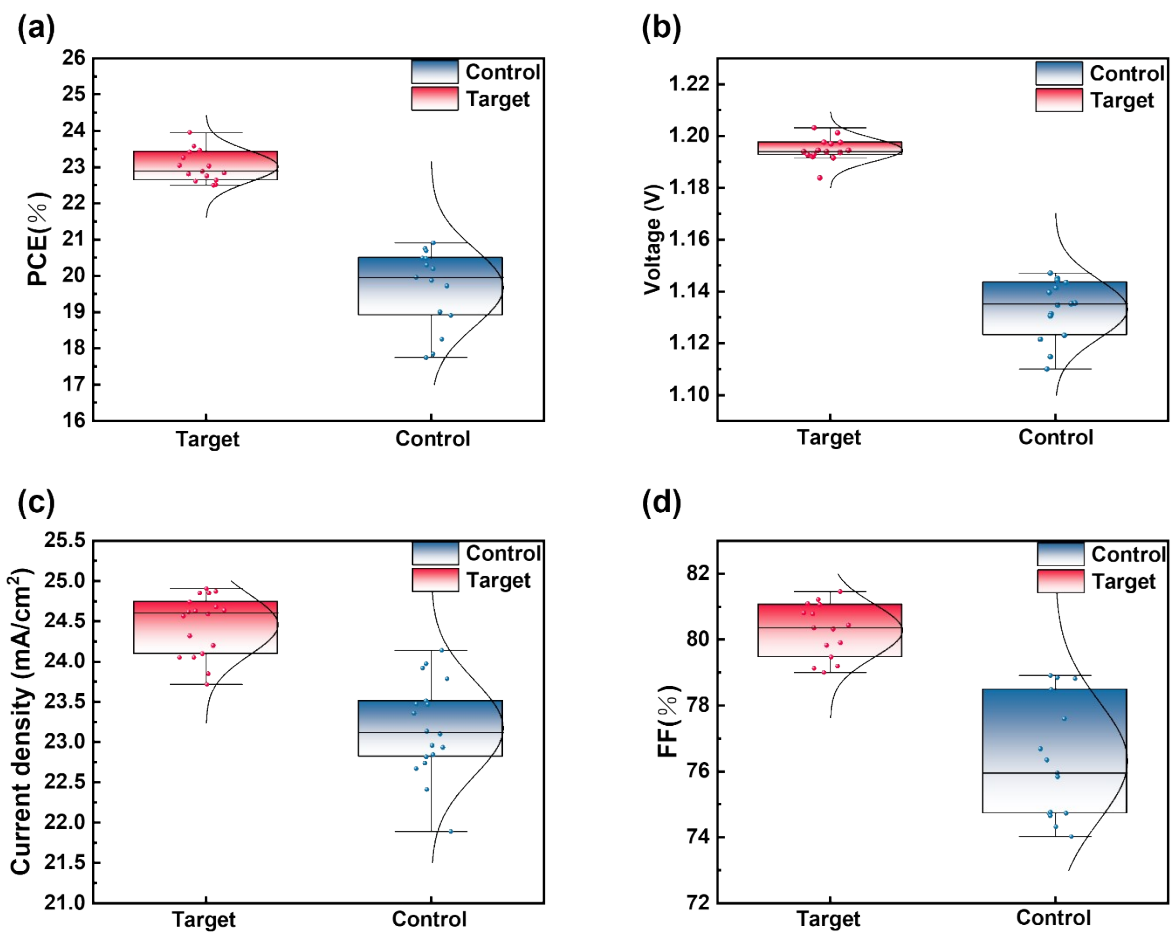


Figure S12. Device performance a) PCE b) V_{OC} c) J_{SC} d) FF distribution of the PVSCs based on control and target perovskite films.

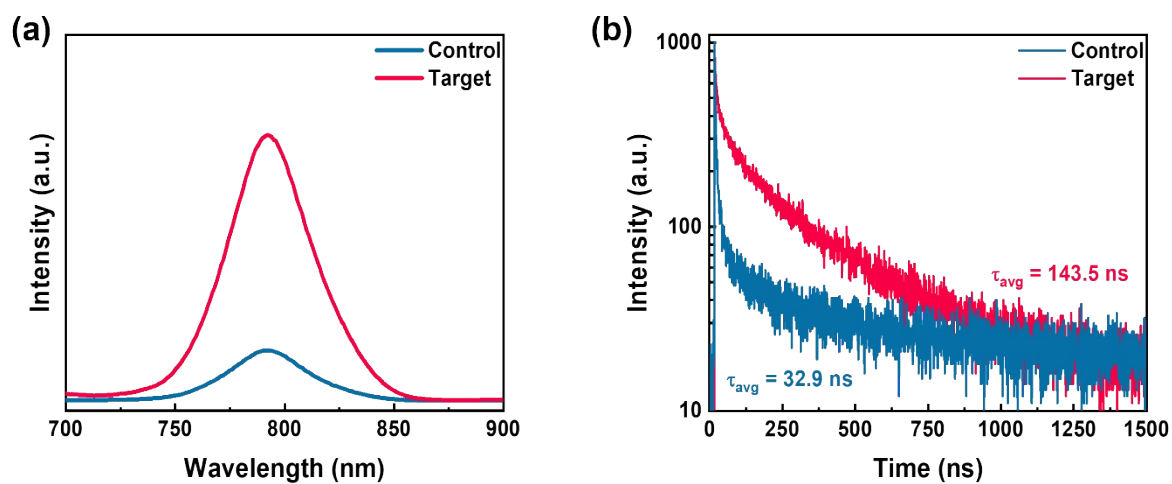


Figure S13. (a) PL spectra and (b) TRPL spectra of the control and target perovskite films.

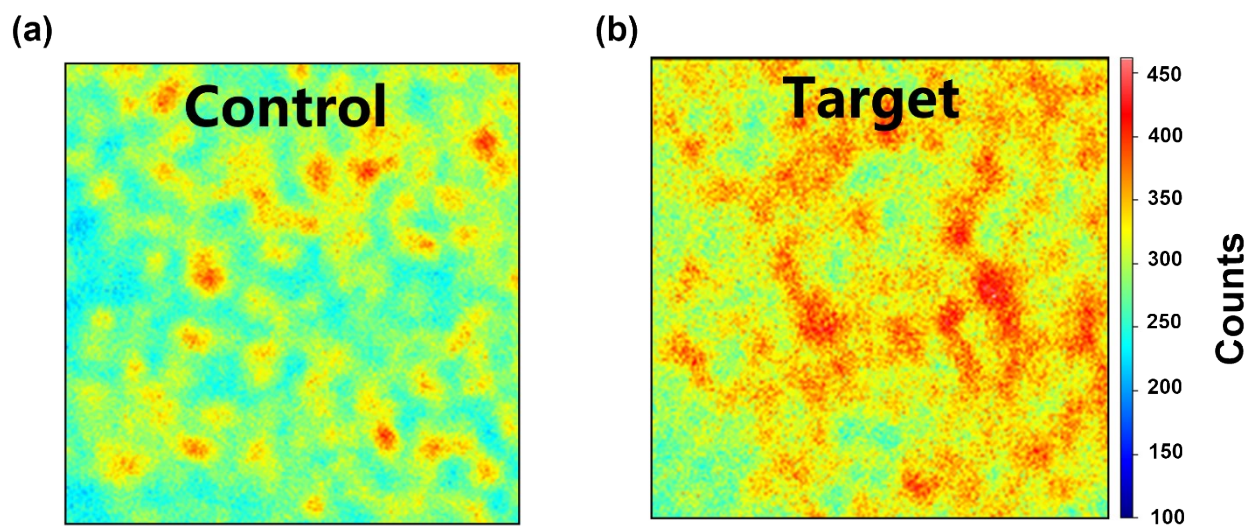


Figure S14. PL mapping under CLSM of the control (a) and target (b) perovskite films.

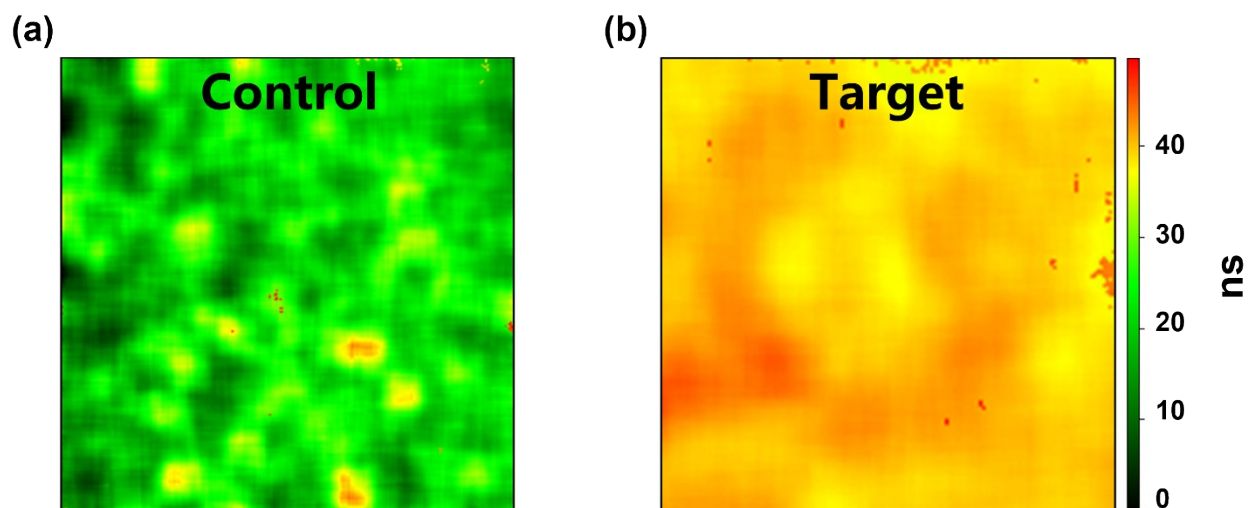


Figure S15. TRPL mapping under CLSM of the control (a) and target (b) perovskite films.

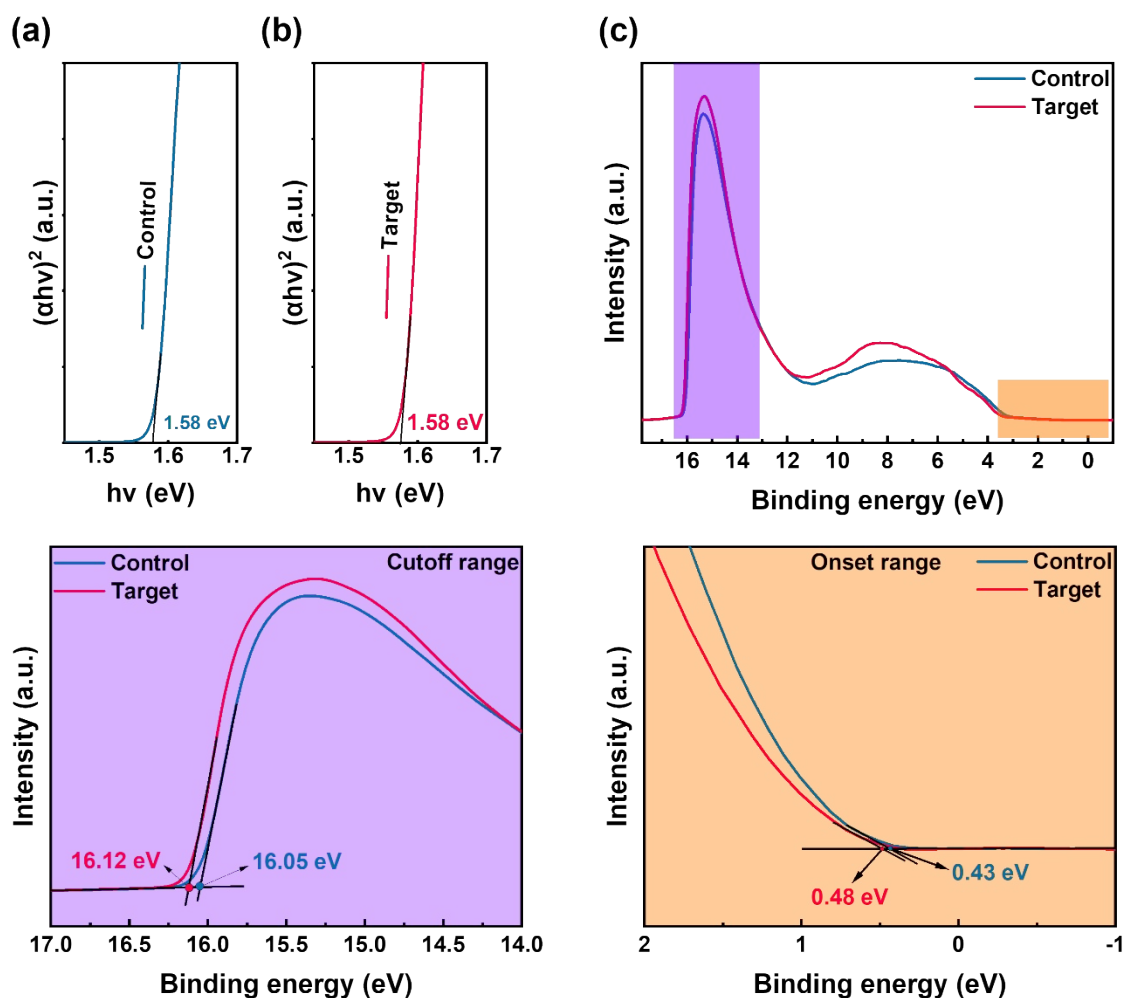


Figure S16. The Tauc plots and Liner of the ultraviolet photoelectron spectroscopy (UPS) results of the (a) control and (b) target perovskite films respectively. (c) Onset and cutoff range from the UPS results. The secondary electron cutoff feature is shifted by the incident photon energy (21.22 eV) to show the position of the vacuum level relative to the Fermi level (located at 0 eV), which corresponds to the work function (WF).

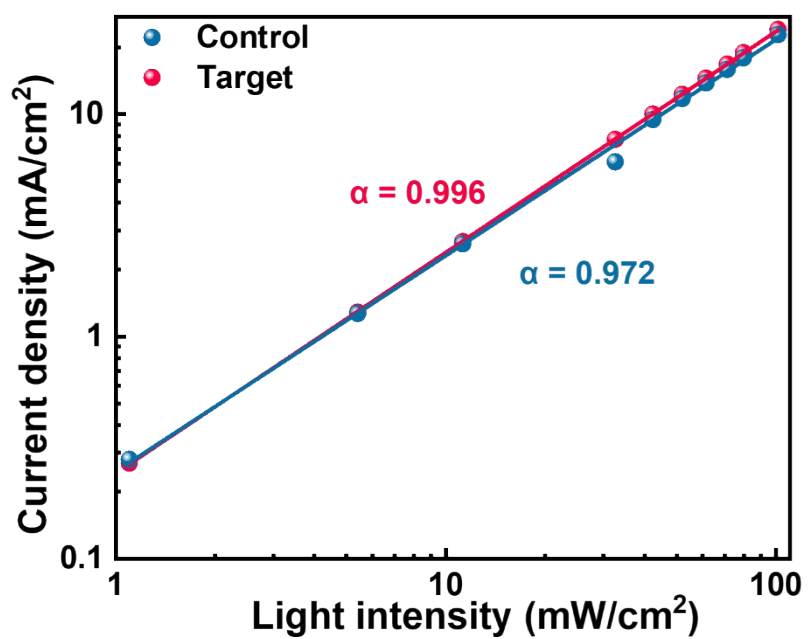


Figure S17. Dependence of J_{SC} at various illumination intensities of the PVSCs based on control and target devices.

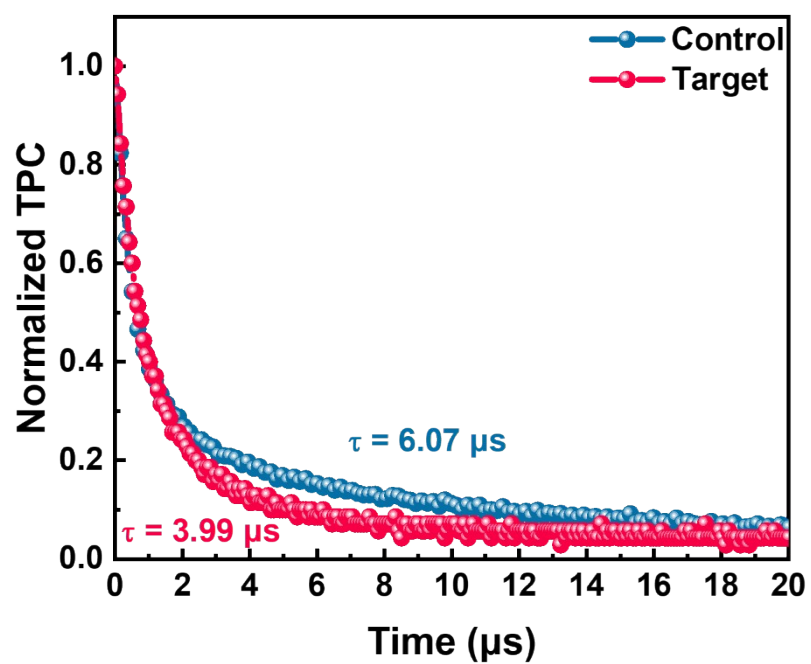


Figure S18. Transient photocurrent decay curves of the PVSCs based on control and target devices.

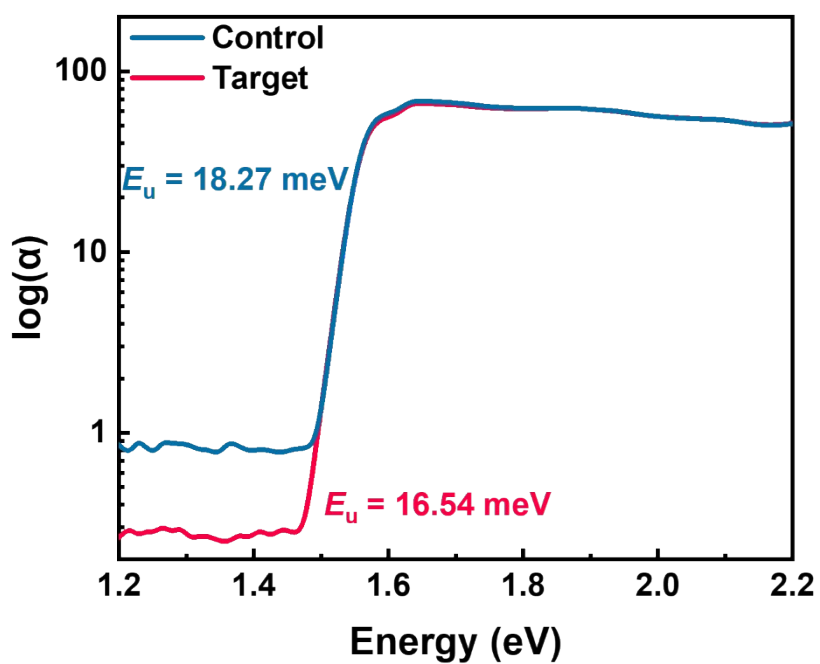


Figure S19. Semilog plot of IPCE at the absorption onset for control and target devices. An Urbach energy (E_u) of 18.27 and 16.54 meV can be obtained from a sharp absorption edge.

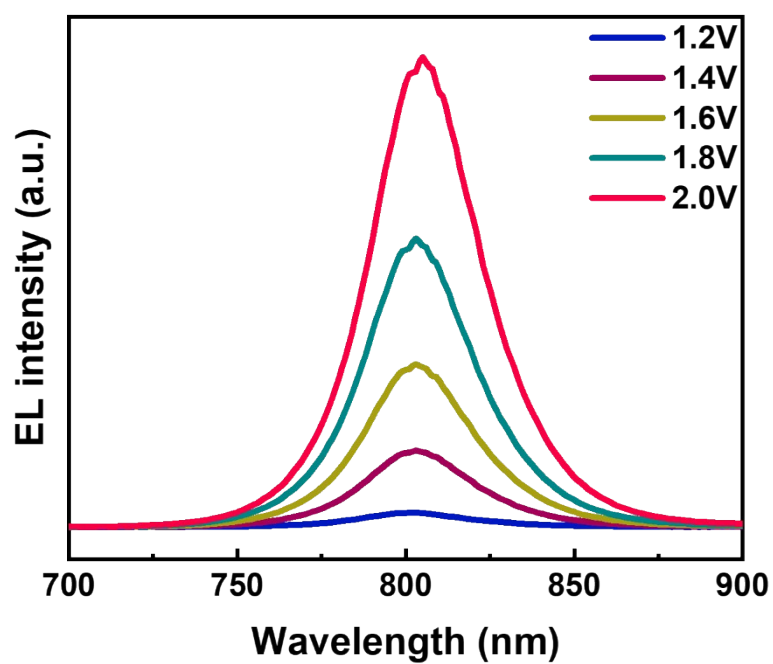


Figure S20. EL spectra of the devices with GluACl under different bias voltages operating as LEDs.

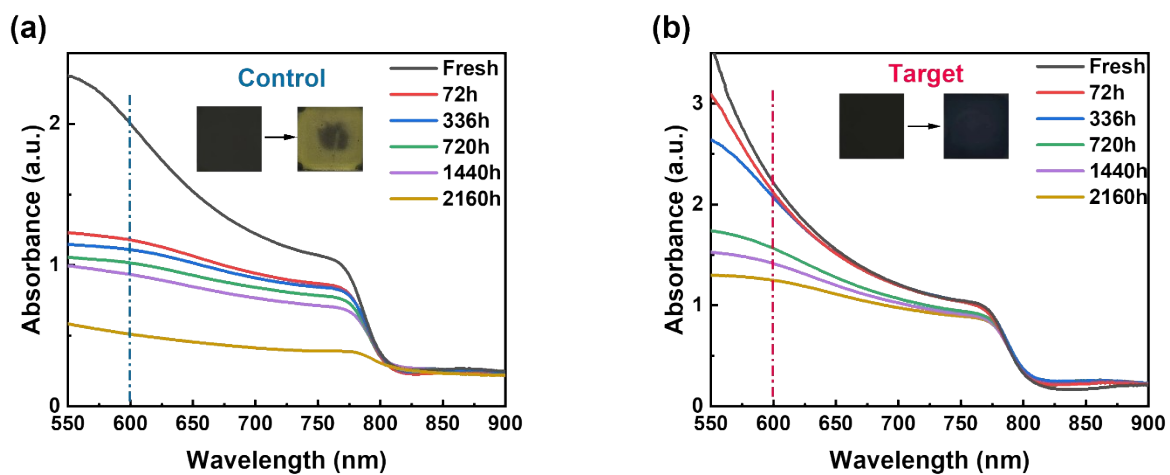


Figure S21. UV-vis absorption evolution of the control (a) and target (b) perovskite films in air ambient (insets are the photographs of the fresh and 2160 h aged perovskite films).

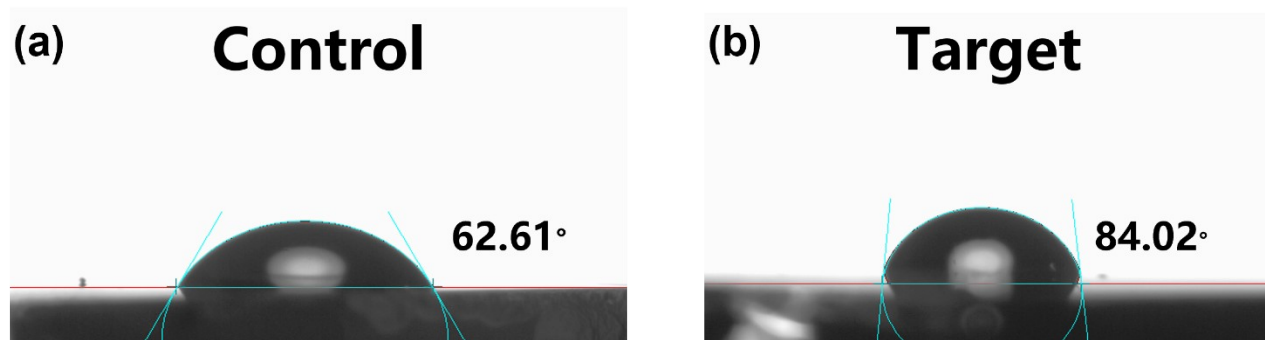


Figure S22. Contact angle measurements based on control (a) and target (b) films.



Figure S23. Photograph of the control and target perovskite films dipped in water.

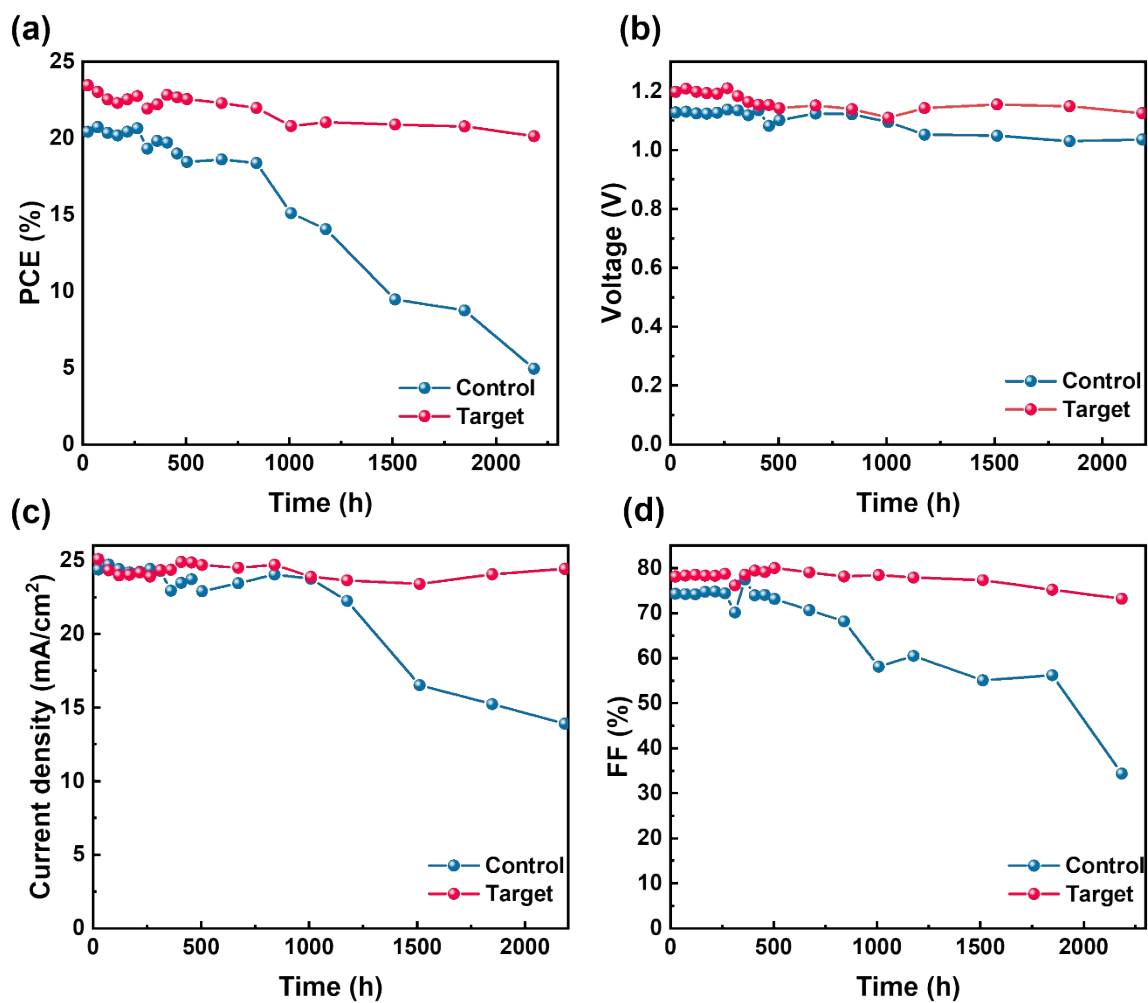


Figure S24. Device performance a) PCE b) V_{OC} c) J_{SC} d) FF evolution over time of the PVSCs based on control and target perovskite films.

Table S1.Crystal data for compound (GluA)(PbI₃)·3DMSO at 298 K.

(GluA)(PbI ₃)·3DMSO	
CCDC	2299758
Empirical formula	C ₁₂ H ₃₁ S ₃ O ₈ NPbI ₃
Formula weight	1001.45
Temperature/K	298
Crystal system	orthorhombic
Space group	<i>P</i> 2 ₁ 2 ₁ 2 ₁
<i>a</i> /Å	8.1488(6)
<i>b</i> /Å	11.5365(9)
<i>c</i> /Å	32.6004(17)
<i>α</i> /°	90
<i>β</i> /°	90
<i>γ</i> /°	90
Volume/Å ³	3064.7(4)
<i>Z</i>	4

Table S2.

Properties of devices prepared with different GluACl doping concentrations.

Sample	V_{oc} (V)	J_{sc} (mA/cm ²)	FF(%)	PCE(%)
Control	1.144	23.93	76.59	20.97
0.05mg GluACl	1.153	24.88	79.47	22.84
0.10mg GluACl	1.203	24.90	79.95	23.96
0.20mg GluACl	1.184	24.24	80.24	23.03

Table S3.

The time-resolved photoluminescence (TRPL) characteristics values of the control and target perovskite films.

Sample	τ_1	τ_2	$A_1(\%)$	$A_2(\%)$	τ_{ave}
Control	9.89	217.45	26.75	73.25	32.90
Target	32.38	290.40	12.85	87.15	143.5

Table S4.

Parameters of the band structure of the control and target perovskite films.

Sample	E_{cutoff} (eV)	E_{onset} (eV)	E_{V}/HOMO (eV)	E_{C}/LUMO (eV)
Control	16.05	0.43	-5.60	-4.02
Target	16.12	0.48	-5.58	-4.00

- S1 (a) P. Giannozzi, S. Baroni, N. Bonini, M. Calandra, R. Car, C. Cavazzoni, D. Ceresoli, G. L. Chiarotti, M. Cococcioni, I. Dabo, A. Dal Corso, S. de Gironcoli, S. Fabris, G. Fratesi, R. Gebauer, U. Gerstmann, C. Gougoussis, A. Kokalj, M. Lazzeri, L. Martin-Samos, N. Marzari, F. Mauri, R. Mazzarello, S. Paolini, A. Pasquarello, L. Paulatto, C. Sbraccia, S. Scandolo, G. Sciauzero, A. P. Seitsonen, A. Smogunov, P. Umari and R. M. Wentzcovitch, *J. Phys.: Condens. Matter*, 2009, **21**, 395502; (b) P. Giannozzi, O. Andreussi, T. Brumme, O. Bunau, M. Buongiorno Nardelli, M. Calandra, R. Car, C. Cavazzoni, D. Ceresoli, M. Cococcioni, N. Colonna, I. Carnimeo, A. Dal Corso, S. de Gironcoli, P. Delugas, R. A. DiStasio, A. Ferretti, A. Floris, G. Fratesi, G. Fugallo, R. Gebauer, U. Gerstmann, F. Giustino, T. Gorni, J. Jia, M. Kawamura, H. Y. Ko, A. Kokalj, E. Küçükbenli, M. Lazzeri, M. Marsili, N. Marzari, F. Mauri, N. L. Nguyen, H. V. Nguyen, A. Otero-de-la-Roza, L. Paulatto, S. Poncé, D. Rocca, R. Sabatini, B. Santra, M. Schlipf, A. P. Seitsonen, A. Smogunov, I. Timrov, T. Thonhauser, P. Umari, N. Vast, X. Wu and S. Baroni, *J. Phys.: Condens. Matter*, 2017, **29**, 465901.
- S2 (a) G. Prandini, A. Marrazzo, I. E. Castelli, N. Mounet and N. Marzari, *npj Computational Materials*, 2018, **4**, 72; (b) K. Lejaeghere, G. Bihlmayer, T. Björkman, P. Blaha, S. Blügel, V. Blum, D. Caliste, I. E. Castelli, S. J. Clark, A. Dal Corso, S. de Gironcoli, T. Deutsch, J. K. Dewhurst, I. Di Marco, C. Draxl, M. Dułak, O. Eriksson, J. A. Flores-Livas, K. F. Garrity, L. Genovese, P. Giannozzi, M. Giantomassi, S. Goedecker, X. Gonze, O. Grånäs, E. K. U. Gross, A. Gulans, F. Gygi, D. R. Hamann, P. J. Hasnip, N. A. W. Holzwarth, D. Iuşan, D. B. Jochym, F. Jollet, D. Jones, G. Kresse, K. Koepnik, E. Küçükbenli, Y. O. Kvashnin, I. L. M. Locht, S. Lubeck, M. Marsman, N. Marzari, U. Nitzsche, L. Nordström, T. Ozaki, L. Paulatto, C. J. Pickard, W. Poelmans, M. I. J. Probert, K. Refson, M. Richter, G.-M. Rignanese, S. Saha, M. Scheffler, M. Schlipf, K. Schwarz, S. Sharma, F. Tavazza, P. Thunström, A. Tkatchenko, M. Torrent, D. Vanderbilt, M. J. van Setten, V. Van Speybroeck, J. M. Wills, J. R. Yates, G.-X. Zhang and S. Cottenier, *Science*, 2016, **351**, aad3000.
- S3 S. Grimme, J. Antony, S. Ehrlich and H. Krieg, *J. Chem. Phys.*, 2010, **132**, 154104.
- S4 (a) F. Neese, *WIREs Computational Molecular Science*, 2022, **12**, e1606; (b) F. Neese, F. Wennmo, U. Becker and C. Riplinger, *J. Chem. Phys.*, 2020, **152**, 224108.
- S5 T. Lu and F. Chen, *J. Comput. Chem.*, 2012, **33**, 580.
- S6 E. F. Pettersen, T. D. Goddard, C. C. Huang, E. C. Meng, G. S. Couch, T. I. Croll, J. H. Morris and T. E. Ferrin, *Protein Sci.*, 2021, **30**, 70.
- S7 (a) E. Artacho, E. Anglada, O. Diéguez, J. D. Gale, A. García, J. Junquera, R. M. Martin, P. Ordejón, J. M. Pruneda, D. Sánchez-Portal and J. M. Soler, *J. Phys.: Condens. Matter*, 2008, **20**, 064208; (b) M. S. José, A. Emilio, D. G. Julian, G. Alberto, J. Javier, O. Pablo and S.-P. Daniel, *J. Phys.: Condens. Matter*, 2002, **14**, 2745.
- S8 Y. Huang, Z. Yuan, J. Yang, S. Yin, A. Liang, G. Xie, C. Feng, Z. Zhou, Q. Xue, Y. Pan, F. Huang and Y. Chen, *Sci. China Chem.*, 2023, **66**, 449.